Proceedings of the ASME 2025 Conference on Smart Materials, Adaptive Structures and Intelligent Systems
SMASIS2025
September 8-10, 2025, St. Louis, MO

SMASIS2025-167940

SPECTROSPATIAL ANALYSIS OF A NONLINEAR HIERARCHICAL ACOUSTIC METAMATERIAL

Ashenafi Abebe Mebrat, Joshua LeGrande, Oumar Barry*
Department of Mechanical Engineering
Virginia Polytechnic Institute and State University
Blacksburg, Virginia 24061

ABSTRACT

Metamaterials are engineered structures designed to manipulate wave propagation according to the design and the intended functionality. Depending on their configuration and input excitation, these materials can behave linearly or nonlinearly. This study theoretically examined the wave propagation behaviors in one-dimensional nonlinear hierarchical metamaterial containing cascaded local resonators. The dispersion relations were determined analytically and numerically validated. The numerical simulation is performed through the MATLAB built-in ode45 integrator excited by unidirectional traveling wave packets. The results show that this hierarchical metamaterial simultaneously excites both the acoustic and optical modes of the dispersion spectrum. The simultaneous presence of both acoustic and optical modes is due to the spatially varying relative motion between the masses. The second optical mode is converted to the first optical and acoustic modes. In addition, hardening nonlinearity transforms the input wave packet to solitary and dispersive waves, while softening generates mainly dispersive wave packets. The nonlinear wave propagation behaviors observed in this study are beneficial for the design of broad-band mechanical energy harvesters, diodes, and sensors.

1 Introduction

Metamaterials, with their engineered structures, are revolutionizing the next generation of technological innovations and developments in the areas of acoustics, electromagnetics, and optics. The research on metamaterials has expanded significantly in recent years. Applications realized through structural metamaterials, such as cloaking [1–3], acoustic black holes [4], and stealth technology [5], are pushing the boundaries beyond the limits of classical materials.

Metamaterial design typically involves the integration of periodic phononic crystals [6] or locally resonant structures [7] to achieve tailored wave manipulation. Nonlinearity is an emerging approach to further improve their functionality by opening up new elastic wave features [8]. In contrast to their linear equivalents, nonlinear metamaterials exhibit unique characteristics such as wave localization [7], amplitude-dependent dispersion [9], pseudo-bandgap, and mode conversion [10, 11]. Nonlinearity can be weak or strong in proportion to the magnitude of the input amplitude [12]. In weak nonlinearity, the effects are small perturbations of the linear behavior, allowing the implementation of approximate analytical methods to derive the dispersion relations [13].

In the propagation of waves, frequency mode conversion is an important phenomenon for altering the input frequency. Incident wave frequency mode conversion enabled the discovery of several wave devices. A frequency up conversion was used to design an acoustic rectifier [14], while designing a mechanical diode takes advantage of the frequency shift [15]. However, due to the relatively weak nonlinear parameters in conventional materials, the resulting converted frequency components typically exhibit lower amplitudes [16]. In addition, such systems are prone to generating unwanted frequency interplay. Alternatively, nonlinear acoustic metamaterials have shown considerable

*Corresponding Author (Email: obarry@vt.edu)

potential to achieve efficient frequency conversion and energy transfer [10].

In the design of monoresonator acoustic metamaterials, nonlinearity has been introduced into the local resonator [17], the chain [15, 18], or both the local resonator and the chain [19]. The chain nonlinearity affects the short-wavelength limit, but local resonator nonlinearity alters the long-wavelength limit, respectively. The nonlinearity applied to the chain and multiple local resonators affects both the long- and short-wavelength regions. A study was conducted on a locally resonant Kresling-origami metamaterial, where nonlinearity was introduced exclusively within the resonator [17]. The results showed a dispersion shift due to nonlinear coupling. The propagation of Hann-modulated transient wave packet was studied in an undamped locally resonant nonlinear acoustic metamaterial [15]. The frequency and wavenumber shifting led to the formation of a pseudo bandgap, which is useful for the design of direction-dependent wave filtering mechanical devices. Nonlinear damped acoustic metamaterials with a single resonator [18] and nonlinear diatomic metamaterials [20], were shown to exhibit damping-dependent variations in the amplitude and shape of the transient wave packet. Nonetheless, an acoustic metamaterial containing a single resonator is less robust in terms of operating range than that of a unit cell containing multiple masses [13].

Recently, a metamaterial consisting of two local resonators arranged in parallel was designed to enable targeted energy transfer through vibro-impact nonlinearity [21]. The vibro-impact mechanism facilitated bidirectional energy transfer (mode conversion) between the lower and higher frequency bands. Moreover, studies are showing that hierarchical metamaterials are capable of generating multiple mode branches [22, 23]. This enables distinct multilevel energy routing, allowing for frequency conversion beyond the excitation band. Recent efforts have focused on the design of hierarchical metamaterials, which offer promising lightweight structures [22]. The band structure of linear pure mechanical [24] and electromechanical [25] light weight hierarchical metamaterials with local resonators organized in outward and inward configurations was investigated. The results revealed that, specific structural configurations plays a critical role in tailoring the band structure.

The need to reduce structural weight while simultaneously enhancing wave propagation characteristics motivates the study of hierarchical nonlinear metamaterials. In this work, we studied the wave propagation behaviors in a nonlinear hierarchical metamaterial containing cascaded nonlinear resonators using analytical and numerical methods. The analytical method is useful to predict the dispersion including cutoff frequencies, whereas the spectrospatial analysis helps to detail distortion and other nonlinear behaviors. Nonlinearities are applied to both the main chain and local resonators to study their effect in all wavelength regions.

2 System Design and Mathematical Modeling

The schematic diagram for the infinite chain is illustrated in Fig. 1. The unit cell of the chain consists of the outer mass m_0, connected to the adjacent cells by linear and nonlinear stiffnesses k_0 and Γ_0, respectively. The local resonators have masses m_1 and m_2 which are connected to the outer mass by linear stiffnesses (k_1, k_2, and k_3) and nonlinear stiffnesses (Γ_1, Γ_2, and Γ_3).

The equation of motion for the j^{th} unit cell is expressed as:

$$m_0\ddot{u}_j + k_0(2u_j - u_{j-1} - u_{j+1}) + k_1(u_j - y_{j1}) + k_3(u_j - y_{j2}) + \varepsilon\Gamma_0\left[(u_j - u_{j-1})^3 + (u_j - u_{j+1})^3\right] + \varepsilon\Gamma_1(u_j - y_{j1})^3 + \varepsilon\Gamma_3(u_j - y_{j2})^3 = 0 \quad (1)$$

$$m_1\ddot{y}_{j1} + k_1(y_{j1} - u_j) + k_2(y_{j1} - y_{j2}) + \varepsilon\Gamma_1(y_{j1} - u_j)^3 + \varepsilon\Gamma_2(y_{j1} - y_{j2})^3 = 0 \quad (2)$$

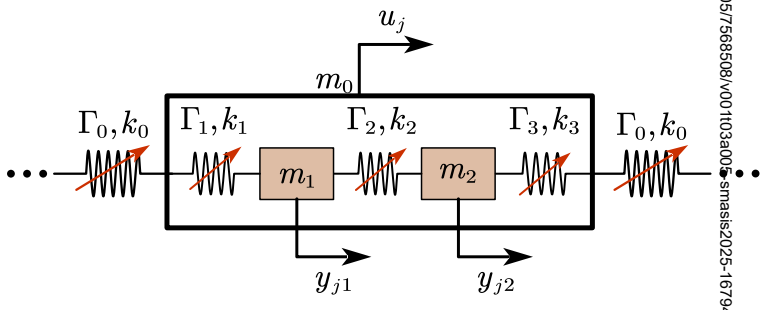

FIGURE 1: Chain of hierarchical nonlinear metamaterial with cascaded resonators.

$$m_2\ddot{y}_{j2} + k_2(y_{j2} - y_{j1}) + k_3(y_{j2} - u_j) + \varepsilon\Gamma_2(y_{j2} - y_{j1})^3 + \varepsilon\Gamma_3(y_{j2} - u_j)^3 = 0 \quad (3)$$

where u_j, y_{j1} and y_{j2} represent the displacements of the outer mass and the local resonators, respectively, and ε is a weak perturbation parameter.

To simplify, dimensionless parameters $\alpha_i = \frac{k_i}{k_0}$, $\gamma_0 = \frac{\Gamma_0}{k_0}$, and $\gamma_i = \frac{\Gamma_i}{k_0}$, are defined by normalizing the stiffness coefficients with

respect to k_0, while $\omega_0^2 = \frac{k_0}{m_0}$ is normalized with respect to m_0. Here, i represents the local resonator stiffness coefficient subscripts 1, 2, and 3. In addition, η and β_1 are the mass ratios defined as $\eta = \frac{m_1+m_2}{m_0}$ and $\beta_1 = \frac{m_1}{m_1+m_2}$, satisfying the relations $m_1 = \eta\beta_1 m_0$ and $m_2 = \eta(1-\beta_1)m_0$. Using dimensionless time $\tau = \omega t$, the differentiation operator can be transformed into the form $\frac{d}{dt} = \omega\frac{d}{d\tau}$, $\frac{d^2}{dt^2} = \omega^2\frac{d^2}{d\tau^2}$, and $\Omega^2 = \frac{\omega^2}{\omega_0^2}$. Then, Equations (1) to (3) reduced to:

$$\Omega^2\frac{\partial^2 u_j}{\partial\tau^2} + (2u_j - u_{j-1} - u_{j+1}) + \varepsilon\gamma_0\left[(u_j - u_{j-1})^3 + (u_j - u_{j+1})^3\right] + \alpha_1(u_j - y_{j1}) + \alpha_3(u_j - y_{j2}) + \varepsilon\gamma_1(u_j - y_{j1})^3 + \varepsilon\gamma_3(u_j - y_{j2})^3 = 0 \tag{4}$$

$$\eta\beta_1\Omega^2\frac{\partial^2 y_{j1}}{\partial\tau^2} + \alpha_1(y_{j1} - u_j) + \alpha_2(y_{j1} - y_{j2}) + \varepsilon\gamma_1(y_{j1} - u_j)^3 + \varepsilon\gamma_2(y_{j1} - y_{j2})^3 = 0 \tag{5}$$

$$\eta(1-\beta_1)\Omega^2\frac{\partial^2 y_{j2}}{\partial\tau^2} + \alpha_2(y_{j2} - y_{j1)}) + \alpha_3(y_{j2} - u_{j)}) + \varepsilon\gamma_2(y_{j2} - y_{j1)})^3 + \varepsilon\gamma_3(y_{j2} - u_j)^3 = 0 \tag{6}$$

The Lindstedt-Poincare weakly nonlinear perturbation method is implemented to derive the approximate dispersion relations [26]. Using this method, the assumed weak perturbation expressions for Ω, u_j, y_{j1}, and y_{j2} are:

$\Omega = \Omega_0 + \varepsilon\Omega_1$, $u_j = u_j^0 + \varepsilon u_j^1$, $y_{j1} = y_{j1}^0 + \varepsilon y_{j1}^1$, and $y_{j2} = y_{j2}^0 + \varepsilon y_{j2}^1$.

Further, assume a plane wave harmonic solutions in the form of Equation (7) [15]:

$$\begin{cases} u_j^0 = \frac{A_0}{2}e^{in\kappa}e^{i\tau} + \text{cc}, \\ y_{j1}^0 = \frac{B_0}{2}e^{in\kappa}e^{i\tau} + \text{cc}, \\ y_{j2}^0 = \frac{C_0}{2}e^{in\kappa}e^{i\tau} + \text{cc}. \end{cases} \tag{7}$$

Here, A_0, B_0 and C_0 are amplitudes of the outer mass, the first and second resonators respectively, and *cc* is the complex conjugate. By substituting the weak perturbation expressions into Equations (4) to (6), performing some algebraic operations, separating terms of order ε^0 and ε^1, and substituting the assumed solutions given in Equation (7), we obtain the linear and nonlinear dispersion Equations (8) and (9), respectively.

$$\alpha_3(\alpha_1\alpha_2 + \alpha_1\alpha_3 + \alpha_2\alpha_3 - \alpha_3\beta_1\eta\Omega_0^2) + [\alpha_1 + \alpha_3 - \eta\Omega_0^2(1-\beta_1)] \times [\alpha_1^2 - (\alpha_1 + \alpha_2 - \beta_1\eta\Omega_0^2)(\alpha_1 + \alpha_3 - \Omega_0^2 + 2(1 - cos(\kappa)))] + \alpha_2[2\alpha_2 + \alpha_1\alpha_2 + \alpha_1\alpha_3 - \alpha_2\Omega_0^2 - 2\alpha_2 cos(\kappa)] = 0 \tag{8}$$

$$[QP(\Omega_0^2\frac{\partial^2}{\partial\tau^2} + \alpha_1 + \alpha_3) - Q\alpha_3^2 - (P\alpha_1 + \alpha_2\alpha_3)^2]u_j^1 + QP[2u_j^1 - u_{j-1}^1 - u_{j+1}^1] = (P\alpha_1 + \alpha_2\alpha_3)(PR_2 + \alpha_2 R_3) + Q(PR_1 + \alpha_3 R_3) \tag{9}$$

The detailed expressions for R_1, R_2, R_3, P and Q are given in the appendix. Expanding the right-hand side of Equation (9) and equating the coefficients of secular forcing terms to zero, the solution for the first-order dimensionless frequency Ω_1 is a function of the zero-order dimensionless frequency, Ω_0 and the wavenumber, κ. Refer to the appendix for the solution of Ω_1. Finally, the corrected weak perturbation dispersion of the nonlinear chain is given as:

$$\Omega^i = \Omega_0^i + \varepsilon\Omega_1^i \tag{10}$$

where superscript i is an integer denoting the i^{th} mode branch.

3 Spectrospatail Wave Analysis Using Analytical and Numerical Methods

The dispersion relations obtained from the analytical method are numerically validated as shown in Fig. 2. To numerically construct the dispersion curves, transient wave analysis is employed. A Hann window transient wave packet is injected into the finite chain consisting of 1500 unit cells. The normalized system parameters used for this study are $\alpha_1 = \alpha_2 = \alpha_3 = 1$, $\beta_1 = 0.75$, $\eta = 1$, and $\omega_0 = 1000$ rad / s. The numerical simulations are conducted using the initial conditions given in Equation (11).

$$\begin{cases} u_j(0) = \dfrac{A_0}{2}\left(H(j-1) - H\left(j-1-\dfrac{2\pi N_{cy}}{\kappa}\right)\right) \\ \qquad\qquad \left(1-\cos\left(\dfrac{j\kappa}{N_{cy}}\right)\right)\sin(j\kappa) \\ \dot{u}_j(0) = \dfrac{A_0}{2}\left(H(j-1) - H\left(j-1-\dfrac{2\pi N_{cy}}{\kappa}\right)\right)U_j \\ y_{j1}(0) = F u_j(0) \\ \dot{y}_{j1}(0) = F\dot{u}_j(0) \\ y_{j2}(0) = J\left(\alpha_3 u_j(0) + \alpha_2 y_{j1}(0)\right) \\ \dot{y}_{j2}(0) = J\left(\alpha_3 \dot{u}_j(0) + \alpha_2 \dot{y}_{j1}(0)\right) \end{cases} \tag{11}$$

In Equation (11), $H(x)$ is the Heaviside function, while N_{cy} is chosen as 7, representing the number of cycles for the Hann-modulated input wave packet. The function U_j defines the unidirectional traveling wave packet, and the constants F and J are given in Equation (13):

$$U_j = \frac{\omega}{N_{cy}}\sin\left(\frac{j\kappa}{N_{cy}}\right)\sin(j\kappa) - \omega\left(1-\cos\left(\frac{j\kappa}{N_{cy}}\right)\right)\cos(j\kappa) \tag{12}$$

$$\begin{cases} F = \dfrac{\alpha_2\alpha_3 + \alpha_1(\alpha_2+\alpha_3+\eta(\beta_1-1)\omega_0^2)}{\alpha_2(\alpha_3-\eta\omega_0^2) - \eta\beta_1\omega_0^2(\alpha_3+\eta(\beta_1-1)\omega_0^2)}, \\ \qquad\qquad +\alpha_1(\alpha_2+\alpha_3+\eta(\beta_1-1)\omega_0^2) \\ J = \dfrac{1}{\alpha_2+\alpha_3+\eta(\beta_1-1)\omega_0^2}. \end{cases} \tag{13}$$

Perfectly matched layers (PML) are applied on both ends of the chain to reduce wave reflection. The profile of the PML damping is chosen as [26]:

$$C(j) = C_{\max}\left(\frac{s}{N_{\text{pml}}}\right)^{dp} \tag{14}$$

where $C_{max} = 2e4$ Ns/m, $dp = 3$, and $N_{pml} = 5$ are used for the numerical simulation. Here, s starts at the beginning of the PML and ends at N_{pml}.

Using ode45 MATLAB built in integrator, the response of the wave packet excitation is determined. A 2D fast Fourier transformation (2D FFT) is applied on the amplitude response matrix to reconstruct the dispersion numerically. In this study, the linear chain is evaluated at $\varepsilon\gamma_0 = \varepsilon\gamma_i = 0$, while the nonlinear hardening and softening chains are evaluated at $\varepsilon\gamma_0 = \varepsilon\gamma_i = 0.06$ and $\varepsilon\gamma_0 = \varepsilon\gamma_i = -0.06$, respectively. The simulation times for the excitations in the acoustic and optical modes are 3 s and 1.5 s, respectively.

Figure 2 shows the dispersion relations obtained from the analytical and numerical analyses. The dispersion relation exhibits three distinct mode branches, with the lower branch representing an acoustic mode and the upper two corresponding to optical modes. The approximate analytical dispersion of a nonlinear hardening chain shifts upward, while the dispersion of a softening nonlinear chain shifts downward from the dispersion of the linear chain. The analytical solution failed to predict the second optical mode (third passband) precisely, due to the significant shifting from the linear curve in this region. The nonlinear dispersion curve shifts considerably, which prevents it from accurately representing the weak nonlinear second optical mode. However, the numerical simulation shows that the dominant frequency of the second optical mode is converted down. In both the linear and nonlinear systems, exciting the chains using the second optical mode converts the dominant frequencies down to the acoustic and first optical modes, as illustrated in Fig. 2. Previous studies have demonstrated that nonlinear acoustic metamaterials are capable of achieving frequency down-conversion [16]. In contrast, the present design reveals that even a linear chain can facilitate the down-conversion of higher-order modes as shown in Fig. 2(a).

The dominant frequencies in the nonlinear chain exhibit greater localization compared to those in the linear chain. Due to mode conversion, the numerical method is unable to accurately capture the dominant frequencies near the bandgap boundaries of the traveling wave packet. The long-wavelength frequencies of the optical modes are converted into the acoustic mode, whereas the short-wavelength frequencies of the acoustic wave shift up to the first optical mode.

When a mid-range wavelength first optical mode wave packet is injected, the dominant frequencies shift toward zero frequency and wavenumber for both types of nonlinearity. Hardening nonlinearity exhibits dominant frequencies in both the long-wavelength and short-wavelength regions of the first optical mode, as shown in Fig. 2(b). As illustrated in Fig. 2(c), the dominant frequencies associated with the first optical mode under softening nonlinearity are predominantly confined to the short-wavelength region. On the basis of the dispersion analysis, it is evident that these hierarchical metamaterials enable both the linear and nonlinear chains to facilitate higher-frequency mode down conversions. Although the approximate analytical solution fails to capture the second optical mode, the numerical simulation is also inadequate in resolving the cutoff frequencies for a traveling wave packet.

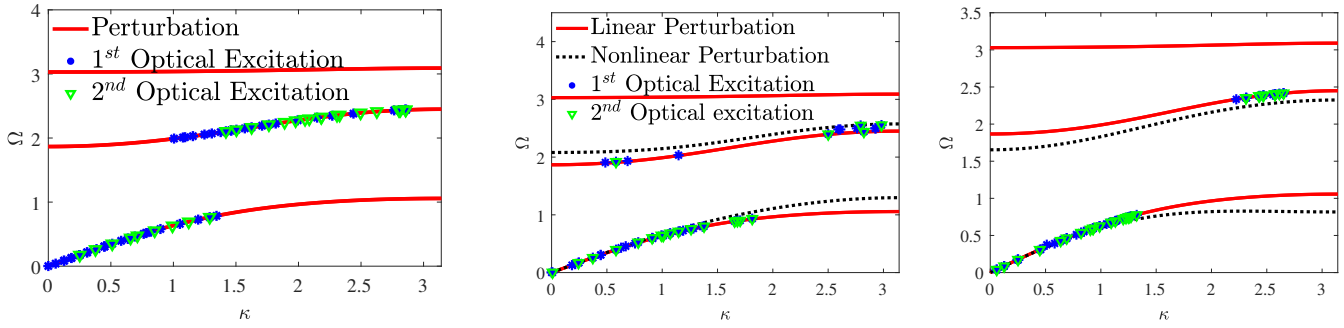

FIGURE 2: Dispersion predicated by analytical and numerical methods at $\beta_1 = 0.75$. (a) linear chain dispersion, (b) nonlinear hardening, and (c) nonlinear softening.

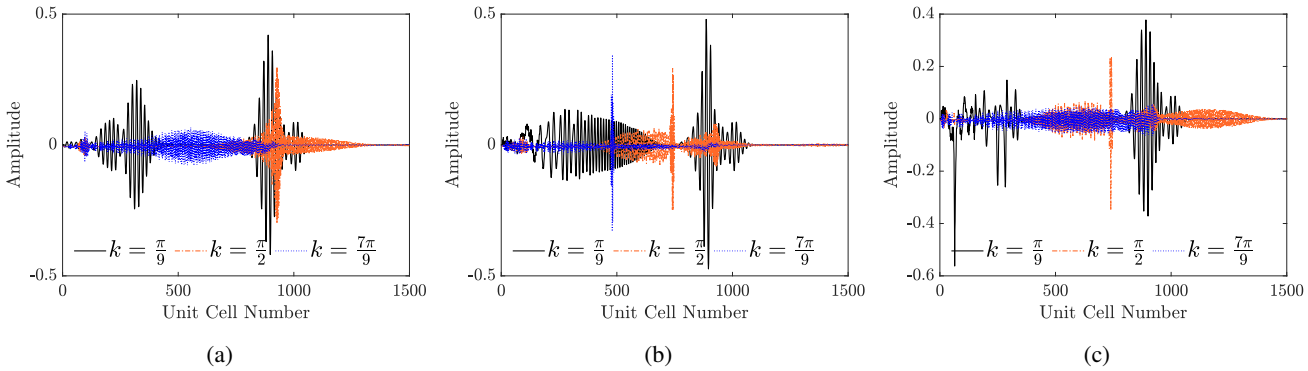

FIGURE 3: Spatial profile at the end of simulation when an acoustic wave packet is injected. (a) linear chain, (b) nonlinear hardening, and (c) nonlinear softening.

3.1 Spectrospatial Behaviors

Unlike linear wave propagation, which maintains its shape, nonlinear wave propagation is characterized by dispersion and distortion [13]. Simple dispersion relations are insufficient to describe these distinctive characteristics. Thus, in this subsection, both the spatial profiles at the end of the simulation and the 2D fast Fourier contours of the traveling waves are provided. The spatial profiles are useful for investigating how the combined nonlinearity of the chain and local resonators changes the shape of the excitation signal during its propagation. Furthermore, the 2D fast Fourier contours reveal unique behaviors such as frequency shift, dispersion, and solitary waves.

3.1.1 Spatial Profile of Transient Wave Packet in Hierarchical Metamaterials

Figure 3 illustrates the spatial profile at the end of the simulation when the input excitation wave packet is in acoustic mode. The long wavelength excitation, $\kappa = \frac{\pi}{9}$, of the linear chain generates two localized wave packets with different amplitudes that travel along the chain in the same direction. The amplitude of the first wave packet is smaller than that of the second wave packet, as shown in Fig. 3(a). In fact, when the chains are excited by the acoustic wave mode, the maximum amplitude of the response is almost half that of the input signal. For medium, $\kappa = \frac{\pi}{2}$, and short, $\kappa = \frac{7\pi}{9}$, wavelength excitations, the shape of the input wave packet is stretched, indicating that the wave packet is distorted. This type of distortion is called dispersive associated distortion [15]. The nonlinear chain distorts the shape of wave packet in all wavelength regions. Hardening and softening nonlinearity mainly distort the first wave packet at the long wavelength, while the second wave packet remains almost undistorted. The hardening nonlinearity at the medium and short wavelength excitation result in dispersive and solitary waves, as shown in Fig. 3(b). The dispersive wave is a distributed low-amplitude wave packet, while the solitary wave is a highly localized high-amplitude wave packet. The softening nonlinearity significantly affects the first wave packet in the long wavelength region. In addition, the solitary wave disappears in the softening

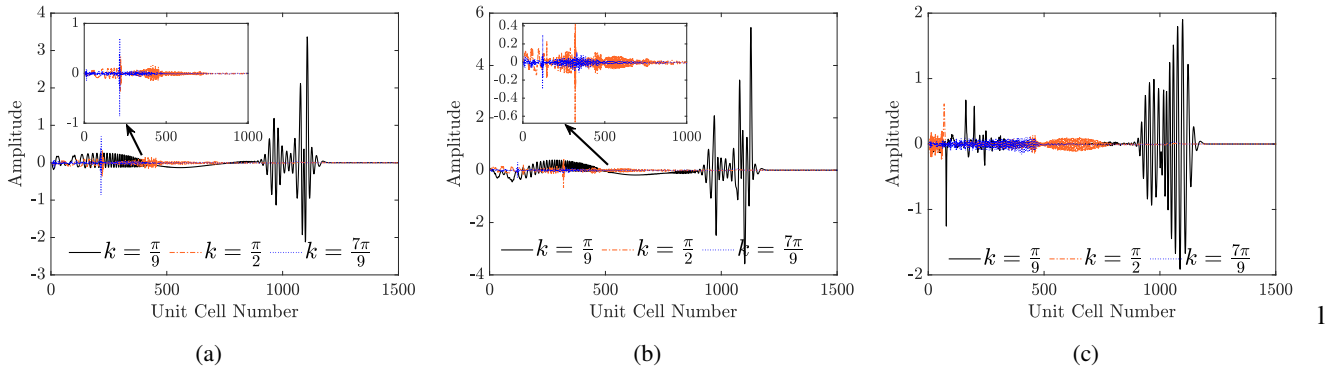

FIGURE 4: Spatial profile at the end of simulation when first optical wave packet is injected. (a) linear chain, (b) nonlinear hardening, and (c) nonlinear softening softening.

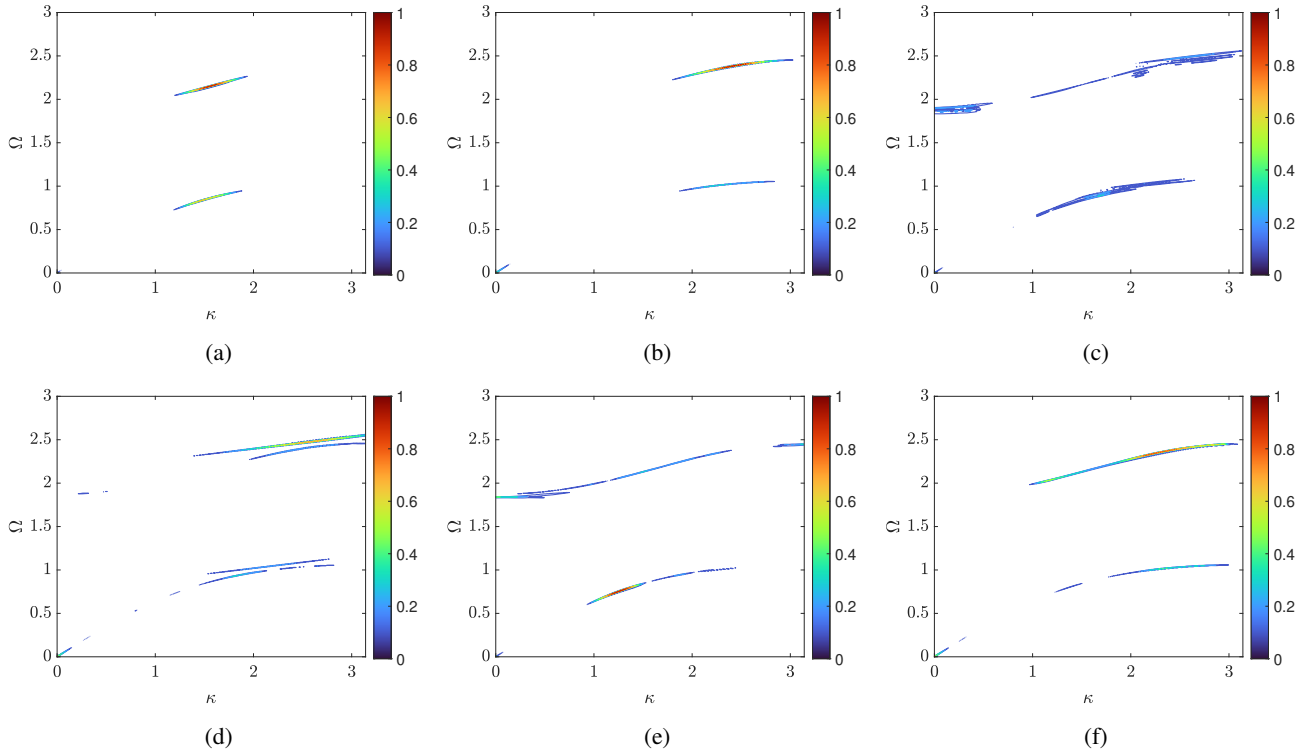

FIGURE 5: 2D-FFT contour when first optical mode wave is injected. (a) linear chain is excited at $\kappa = \frac{\pi}{2}$, (b) linear chain is excited at $\kappa = \frac{7\pi}{9}$, (c) nonlinear hardening excited at $\kappa = \frac{\pi}{2}$, (d) nonlinear hardening excited at $\kappa = \frac{7\pi}{9}$, (e) nonlinear softening excited at $\kappa = \frac{\pi}{2}$, and (f) nonlinear softening excited at $\kappa = \frac{7\pi}{9}$

for a short-wavelength wave, as demonstrated in Fig. 3(c).

The spatial profile of the wave packet propagation excited by the optical mode at the end of the simulations is provided in Fig. 4. Wave packets in all wavelength limits are distorted when the chain is excited by an optical mode branch. The spatial profiles are generated by using the first optical mode excitation, since the second optical mode excitation offers nearly similar spatial profiles. The propagation of long-wavelength wave packets in linear and hardening nonlinear chains shows distortion. It first exhibits a spatially decreasing amplitude followed by a localized wave packet with a higher amplitude, as shown in Figs. 4(a) and 4(b). At medium and short wavelengths, dispersive and soli-

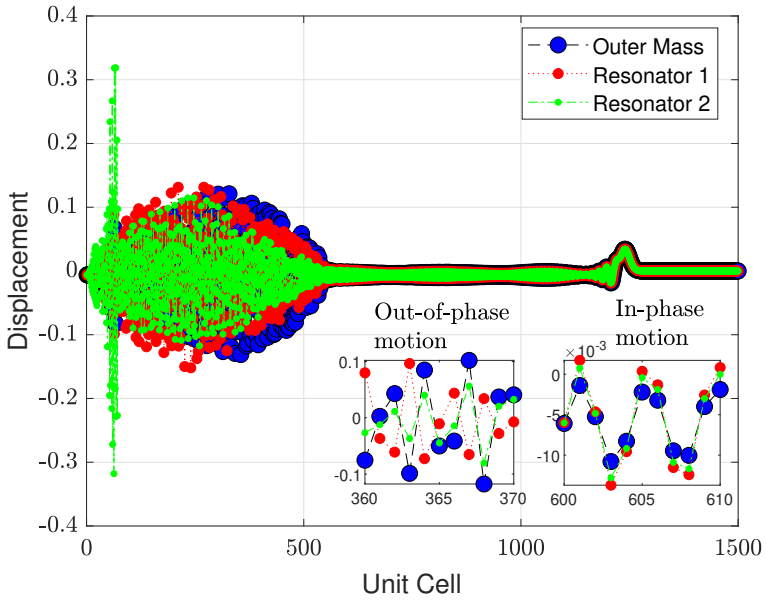

FIGURE 6: The relative motion of outer mass and resonators in the linear chain at the end of the simulation excited by the short wavelength first optical mode.

tary waves characterize the spatial profile in linear and nonlinear hardening cases. The softening of the nonlinear chain generates dispersive and solitary wave packets for medium-wavelength excitation, while only dispersive waves propagate in the short-wavelength regime. The long wavelength is nearly undistorted, as shown in Fig. 4(c). The spatial profiles reveal that hardening nonlinearity localize and disperse the wave packets, while softening primarily gives dispersive wave packet.

3.1.2 Spectral Characterization of the Transient Wave Packets

In this subsection, the spectral features of the transient wave packet are explored in the vicinity of the carrier wavenumber and frequency of the excitation wave packet. The contour lines are the magnitude of the spectral amplitude as a function of κ and Ω for linear and different types of nonlinearities. Given the significant influence of dispersion and nonlinearity on optical modes, this subsection examines the 2D-FFT contour of optical modes.

The 2D-FFT contour shown in Fig. 5, illustrates the dispersion curve when the chain is excited by a first optical mode branch. The applied excitation causes both types of wave mode, acoustic and optical, to be present in the system. The optic-acoustic coupling is attributed to the spatially varying relative motion of the local resonators with respect to the outer mass moving down the chain, as shown in Fig. 6. The first optical mode is observed when the relative motion of one of the resonators is out of phase with the outer mass. The relative motion of resonator 1 is out of phase, for instance, for the unit cells 360 to 370, reflecting the behavior of the first optical mode. There is a transition from the out-of-phase motion to the in-phase motion moving down the chain, resulting in acoustic mode.

The contour shown in Fig. 5(a) displays the optical and acoustic mode branches when the linear chain is excited by the medium-wavelength first optical mode. The shape of these modes are undistorted. The shape of the optical mode is nearly straight with a higher magnitude, indicating that it is a solitary wave packet [15], while the acoustic mode evolves as a weak dispersive wave packet. When the linear chain is excited by a short-wavelength first optical mode branch, both the optical and the acoustic modes stretched more, as shown in Fig. 5(b). The propagation of short-wavelength wave packet in the linear chain is distorted by the dispersion effect. The optical mode branch contains the dominant frequency components under both medium- and short-wavelength excitations of the linear chain.

The dispersion of the medium-wavelength first optical mode in the hardening nonlinear chain is shown in Fig. 5(c). Due to the significant frequency shift, only weak acoustic and first optical mode branches propagate as shown in Fig. 5(c). However, nonlinear hardening provides dispersive and solitary waves in both the acoustic and first optical modes when excited by the short-wavelength wave packet as displayed in Fig. 5(d). The dominant frequency is noted in the solitary wave of the first optical mode, which is observed in the neighborhood of the short wavelength region as well. The dispersive wave of the acoustic mode is very

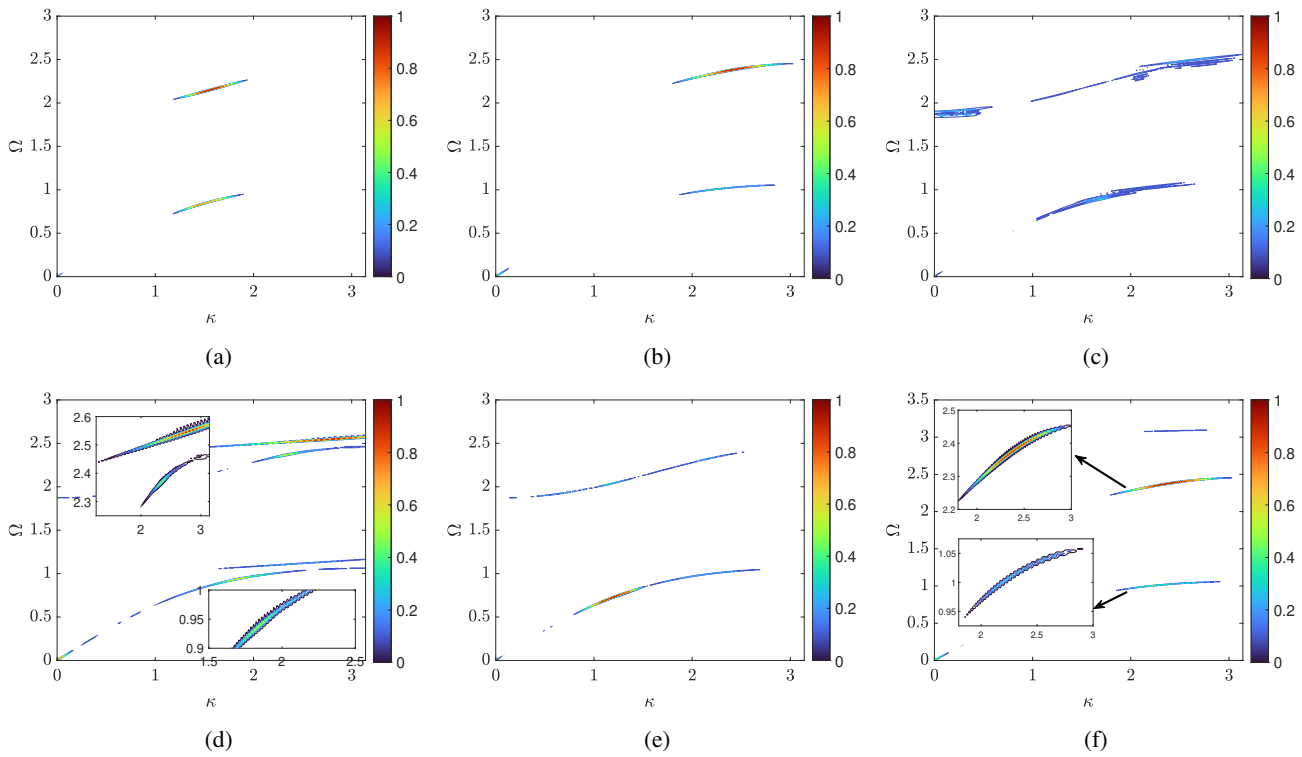

FIGURE 7: 2D-FFT contour when second optical mode wave is injected. (a) linear chain excited at $\kappa = \frac{\pi}{2}$, (b) linear chain excited at $\kappa = \frac{7\pi}{9}$, (c) nonlinear hardening excited at $\kappa = \frac{\pi}{2}$, (d) nonlinear hardening excited at $\kappa = \frac{7\pi}{9}$, (e) nonlinear softening excited at $\kappa = \frac{\pi}{2}$, and (f) nonlinear softening excited at $\kappa = \frac{7\pi}{9}$.

weak in the long-wavelength region. Hardening nonlinearity induces both localization and dispersion in the acoustic and optical mode branches under short-wavelength excitation.

Exciting the nonlinear softening chain using the first optical mode in the medium wavelength results in dominant frequency down conversion, as shown in Fig. 5(e). The softening nonlinearity allows the propagation of dispersive waves in the acoustic and optical modes. The propagation of weak dispersive first optical mode covers almost all wavelength regions, while the acoustic mode is restricted in the medium-range wavelength region. The short wavelength excitation, on the other hand, does not convert down the dominant frequency. Instead, the dominant frequency remains in the short-wavelength region of the first optical mode, as shown in Fig. 5(f). The first optical mode ranges in the medium- and short-wavelength frequency, while the weak dispersive acoustic mode is mainly noted in the short-wavelength limit. However, in hardening nonlinearity, there is mode conversion and wave localization.

Figure 7 illustrates the 2D-FFT contours obtained from the second optical mode wave packet excitation. Under excitation corresponding to the second optical mode, both resonators initially oscillate out of phase with the outer mass at the beginning of the chain. As the wave packet continues to propagate, the system undergoes a relative motion reconfiguration, which leads to the conversion of the high-frequency mode to the low-frequency modes. This is the reason why the system provides the first optical and acoustic modes at the end of the simulation.

The dispersion curves obtained from the excitation of the second optical mode are nearly the same as the 2D-FFT contour obtained from the excitation using the first optical mode. One of the differences observed is that exciting the softening chain using the medium-wavelength second optical mode provides a more stretched acoustic mode, as seen in Fig. 6(e). In contrast, exciting the chain using the medium-wavelength first optical mode results in a less stretched acoustic mode, as shown in Fig. 5(e). Further, when the second optical mode is converted down, there is weak third-mode propagation.

The wave packet propagation behaviors, such as frequency shift and frequency down conversion, observed in this nonlinear hierarchical system, can be used for the design of sensors and directional mechanical wave devices. Optic-acoustic spatial mode coupling is also beneficial for localized vibrational energy harvesting using conventional piezoelectric energy harvesters.

4 CONCLUSION

In this work, the behavior of wave propagation in nonlinear hierarchical medium is predicted using approximate analytical and numerical approaches. The results indicated that hierarchical metamaterials with cascaded local resonators can facilitate the simultaneous propagation of both acoustic and optical modes when the chain is excited by a traveling wave packet. Furthermore, the numerical simulation showed that when the chain is excited using the second optical mode, the input wave packet is converted to lower harmonic modes. The spatial profiles revealed a region with a relatively low amplitude dispersive wave and localized high amplitude waves. These observations are further supported by the 2D-FFT contour, and they are more clearly visible in the 2D-FFT contour. The 2D-FFT contour indicates the concurrent propagation of low-frequency acoustic and high-frequency optical modes. This study theoretically demonstrates the significance of cascaded local resonators in manipulating wave propagation characteristics in nonlinear acoustic metamaterials for localized wave control.

ACKNOWLEDGEMENTS

This work is supported in part by the National Science Foundation (NSF) Grant CMMI-2038187.

REFERENCES

[1] Chen, H., and Chan, C. T., 2010. "Acoustic cloaking and transformation acoustics". *Journal of Physics D: Applied Physics,* ***43***(11), p. 113001.

[2] Li, P., Yang, F., Wang, P., Zhao, J., and Zhong, Z., 2022. "A novel design scheme for acoustic cloaking of complex shape based on region partitioning and multi-origin coordinate transformation". *Applied Mathematics and Mechanics,* ***43***(11), pp. 1641–1656.

[3] Alitalo, P., and Tretyakov, S., 2009. "Electromagnetic cloaking with metamaterials". *Materials today,* ***12***(3), pp. 22–29.

[4] Pelat, A., Gautier, F., Conlon, S. C., and Semperlotti, F., 2020. "The acoustic black hole: A review of theory and applications". *Journal of Sound and Vibration,* ***476***, p. 115316.

[5] Joy, V., Dileep, A., Abhilash, P., Nair, R. U., and Singh, H., 2021. "Metasurfaces for stealth applications: A comprehensive review". *Journal of Electronic Materials,* ***50***(6), pp. 3129–3148.

[6] Boechler, N., Theocharis, G., and Daraio, C., 2011. "Bifurcation-based acoustic switching and rectification". *Nature materials,* ***10***(9), pp. 665–668.

[7] Fang, X., Lacarbonara, W., and Cheng, L., 2024. "Advances in nonlinear acoustic/elastic metamaterials and metastructures". *Nonlinear Dynamics*, pp. 1–28.

[8] Failla, G., Marzani, A., Palermo, A., Russillo, A. F., and Colquitt, D., 2024. Current developments in elastic and acoustic metamaterials science.

[9] Bae, M. H., and Oh, J. H., 2020. "Amplitude-induced bandgap: New type of bandgap for nonlinear elastic metamaterials". *Journal of the Mechanics and Physics of Solids,* ***139***, p. 103930.

[10] Moussatov, A., Castagnède, B., and Gusev, V., 2002. "Frequency up-conversion and frequency down-conversion of acoustic waves in damaged materials". *Physics Letters A,* ***301***(3-4), pp. 281–290.

[11] Jhang, K.-Y., 2009. "Nonlinear ultrasonic techniques for nondestructive assessment of micro damage in material: a review". *International journal of precision engineering and manufacturing,* ***10***, pp. 123–135.

[12] Fronk, M. D., Fang, L., Packo, P., and Leamy, M. J., 2023. "Elastic wave propagation in weakly nonlinear media and metamaterials: a review of recent developments". *Nonlinear Dynamics,* ***111***(12), pp. 10709–10741.

[13] Bukhari, M., and Barry, O., 2020. "Spectro-spatial analyses of a nonlinear metamaterial with multiple nonlinear local resonators". *Nonlinear Dynamics,* ***99***(2), pp. 1539–1560.

[14] Ma, C., Parker, R. G., and Yellen, B. B., 2013. "Optimization of an acoustic rectifier for uni-directional wave propagation in periodic mass–spring lattices". *Journal of Sound and Vibration,* ***332***(20), pp. 4876–4894.

[15] Zhou, W., Li, X., Wang, Y., Chen, W., and Huang, G., 2018. "Spectro-spatial analysis of wave packet propagation in nonlinear acoustic metamaterials". *Journal of Sound and Vibration,* ***413***, pp. 250–269.

[16] Jeon, G. J., and Oh, J. H., 2021. "Nonlinear acoustic metamaterial for efficient frequency down-conversion". *Physical Review E,* ***103***(1), p. 012212.

[17] Yu, X., and Wang, L., 2024. "Wave propagation in nonlinear locally coupled resonant kresling origami metamaterials". *Nonlinear Dynamics*, pp. 1–22.

[18] Liu, M., and Zhou, F., 2024. "Spectro-spatial analysis of nonlinear wave propagation behaviors in damped acoustic metamaterial systems". *Journal of Vibration Engineering & Technologies,* ***12***(1), pp. 53–65.

[19] Bukhari, M., and Barry, O., 2023. "Broadband electromechanical diode: acoustic non-reciprocity in weakly nonlinear metamaterials with electromechanical resonators". *Journal of Vibration and Acoustics,* ***145***(2), p. 021003.

[20] Liu, M., and Xia, B., 2024. "Research on new wave behavior and mechanisms in nonlinear diatomic acoustic metamaterials with linear damping". *Nonlinear Dynamics,* ***112***(1), pp. 403–417.

[21] Al-Sheyyab, M. A., and Bukhari, M. A., 2024. "Unlocking targeted energy transfer in phononic lattices: Exploring local vibro-impact nonlinearity in multiple local resonator metamaterials". *IFAC-PapersOnLine,* ***58***(28), pp. 228–

233.
[22] Xu, X., Barnhart, M. V., Li, X., Chen, Y., and Huang, G., 2019. "Tailoring vibration suppression bands with hierarchical metamaterials containing local resonators". *Journal of Sound and Vibration,* ***442***, pp. 237–248.
[23] Mebrat, A., LeGrande, J., and Barry, O., 2024. "Analytical investigation of electromechanically coupled hierarchical metamaterials for simultaneous vibration attenuation and energy harvesting". In International Design Engineering Technical Conferences and Computers and Information in Engineering Conference, Vol. 88452, American Society of Mechanical Engineers, p. V011T11A007.
[24] Liang, X., Zhang, F., and Jiang, J., 2022. "Ultra-wideband outward-hierarchical metamaterials with graded design". *International Journal of Mechanics and Materials in Design,* ***18***(1), pp. 169–184.
[25] Mebrat, A. A., LeGrande, J., and Barry, O., 2025. "Analytical investigation of electromechanical hierarchical metamaterials for vibration attenuation and energy harvesting". *Applied Sciences,* ***15***(7), p. 3464.
[26] Narisetti, R. K., Leamy, M. J., and Ruzzene, M., 2010. "A perturbation approach for predicting wave propagation in one-dimensional nonlinear periodic structures".

Appendix A: Expression of Constants

$$R_1 = -2\Omega_0\Omega_1\frac{\partial^2 u_j^0}{\partial\tau^2} - \gamma_0\left[(u_j^0-u_{j-1}^0)^3+(u_j^0-u_{j+1}^0)^3\right] - \gamma_1(u_j^0-y_{j1}^0)^3 - \gamma_3(u_j^0-y_{j2}^0)^3 \tag{15}$$

$$R_2 = -2\eta\beta_1\Omega_0\Omega_1\frac{\partial^2 y_{j1}^0}{\partial\tau^2} - \gamma_1(y_{j1}^0-u_j^0)^3 - \gamma_2(y_{j1}^0-y_{j2}^0)^3 \tag{16}$$

$$R_3 = -2\eta(1-\beta_1)\Omega_0\Omega_1\frac{\partial^2 y_{j2}^0}{\partial\tau^2} - \gamma_2(y_{j2}^0-y_{j1)}^0) - \gamma_3(y_{j2}^0-u_{j)}^0) \tag{17}$$

$$P = \eta(1-\beta_1)\Omega_0^2\frac{\partial^2}{\partial\tau^2} + \alpha_1 + \alpha_3 \tag{18}$$

$$Q = P(\eta\beta_1\Omega_0^2\frac{\partial^2}{\partial\tau^2} + \alpha_1 + \alpha_3) - \alpha_2^2 \tag{19}$$

$$\Omega_1 = \frac{X}{Y} \tag{20}$$

$$\begin{aligned}X = {} & 3(\alpha_1+\alpha_3+\eta(-1+\beta_1)\omega_0^2)\\ & \Big[\alpha_1^2\Big(16A_0^3\sin^4(k/2)\gamma_0+(B_0-C_0)^3\gamma_2-(A_0-C_0)^3\gamma_3\Big)\\ & +\alpha_2^2\Big(-16A_0^3\sin^4(k/2)\gamma_0-(A_0-B_0)^3\gamma_1+(A_0-C_0)^3\gamma_3\Big)\\ & +\alpha_2\Big(2\alpha_3\Big(8A_0^3\sin^4(k/2)\gamma_0-(A_0-C_0)^3\gamma_3\Big)\\ & +\eta(-1+\beta_1)\Big(16A_0^3\sin^4(k/2)\gamma_0+(A_0-B_0)^3\gamma_1-\\ & (A_0-C_0)^3\gamma_3\Big)\omega_0^2\Big)\\ & +\eta\beta_1\omega_0^2\Big[\alpha_3\Big(-16A_0^3\sin^4(k/2)\gamma_0-(A_0-B_0)^3\gamma_1+B_0^3\gamma_2\\ & -3B_0^2C_0\gamma_2+3B_0C_0^2\gamma_2-C_0^3\gamma_2+2A_0^3\gamma_3-6A_0^2C_0\gamma_3\\ & +6A_0C_0^2\gamma_3-2C_0^3\gamma_3\Big)\\ & +\eta(-1+\beta_1)\Big(-16A_0^3\sin^4(k/2)\gamma_0-(A_0-B_0)^3\gamma_1+\\ & (A_0-C_0)^3\gamma_3\Big)\omega_0^2\Big]+\alpha_1\Big[2\alpha_3\Big(8A_0^3\sin^4(k/2)\gamma_0-(A_0-C_0)^3\gamma_3\Big)\\ & +\alpha_2\Big(16A_0^3\sin^4(k/2)\gamma_0+(A_0-B_0)^3\gamma_1-B_0^3\gamma_2\\ & +3B_0^2C_0\gamma_2-3B_0C_0^2\gamma_2+C_0^3\gamma_2-2A_0^3\gamma_3+6A_0^2C_0\gamma_3\\ & -6A_0C_0^2\gamma_3+2C_0^3\gamma_3\Big)\\ & +\eta\Big(-16A_0^3\sin^4(k/2)\gamma_0-B_0^3\gamma_2+3B_0^2C_0\gamma_2-3B_0C_0^2\gamma_2+C_0^3\gamma_2\\ & +\beta_1\Big(-(A_0-B_0)^3\gamma_1+(B_0-C_0)^3\gamma_2\Big)+A_0^3\gamma_3-3A_0^2C_0\gamma_3+\\ & 3A_0C_0^2\gamma_3-C_0^3\gamma_3\Big)\omega_0^2\Big]\Big]\end{aligned} \tag{21}$$

$$\begin{aligned}Y = {} & 2\omega_0(\alpha_1+\alpha_3+\eta(-1+\beta_1)\omega_0^2)\Big[-A_0\alpha_2^2+\alpha_1^2(A_0+B_0\eta\beta_1)\\ & +\alpha_2\Big(\alpha_3(A_0+C_0\eta+(B_0-C_0)\eta\beta_1)+A_0\eta(-1+\beta_1)\omega_0^2\Big)\\ & -\eta\beta_1\omega_0^2\Big(\alpha_3(A_0+C_0\eta-C_0\eta\beta_1)+A_0\eta(-1+\beta_1)\omega_0^2\Big)\\ & +\alpha_1\Big(\alpha_3(A_0+C_0\eta+(B_0-C_0)\eta\beta_1)+\alpha_2(A_0+C_0\eta-C_0\eta\beta_1)\\ & +\eta(-A_0-B_0\eta\beta_1+B_0\eta\beta_1^2)\omega_0^2\Big)\Big]\end{aligned} \tag{22}$$